THE JOURNAL OF PHYSICAL CHEMISTRY C

Article

pubs.acs.org/JPCC

Electronic Band Structures of Molybdenum and Tungsten Dichalcogenides by the *GW* Approach

Hong Jiang*

Beijing National Laboratory for Molecular Sciences, State Key Laboratory of Rare Earth Materials Chemistry and Applications, Institute of Theoretical and Computational Chemistry, College of Chemistry and Molecular Engineering, Peking University, 100871 Beijing, China

Supporting Information

ABSTRACT: Molybdenum and tungsten dichalcogenides, MX_2 (M = Mo and W; X = S and Se), characterized by their quasi-two-dimensional layered structure, have attracted intensive interest due to their intriguing physical and chemical properties. In this work, quasi-particle electronic properties of these materials are investigated by many-body perturbation theory in the *GW* approximation, currently the most accurate first-principles approach for electronic band structure of extended systems. It is found that the fundamental band gaps of all of these materials can be well described by the *GW* approach, and the calculated density of states from *GW* quasi-particle band energies agree very well with photoemission spectroscopy data. Ionization potentials of these materials are also studied by combining the slab model using density functional theory and *GW* correction. On the basis of our theoretical findings, we predict that none of the materials in MX_2 (M = Zr, Hf, Mo, and W; X = S and Se) in their bulk form can be directly used as the photocatalyst for overall photosplitting of water because their VBM and CBM energies do not match the redox potentials of water oxidation and reduction, which, however, can be changed by forming nanostructures, especially for MoS_2.

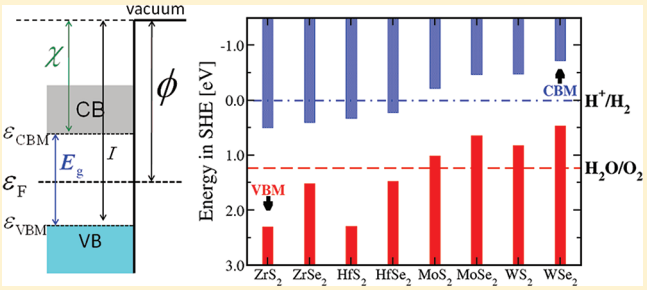

INTRODUCTION

Molybdenum and tungsten disulfide and diselenide MX_2 (M = Mo and W; X = S and Se), often termed as the MoS_2 family, as important members of layered transition-metal dichalcogenides (TMDCs),[1,2] have attracted a lot of interest recently because of their intriguing chemical and physical properties.[3−5] These materials have band gaps falling in the visible or near-infrared light regime so that they are promising for efficient solar-energy conversion.[5] More importantly, the peculiar layered structure of these materials makes it possible to fine tune their electronic properties by either introducing foreign atoms or molecules between weakly bonded layers to form various intercalated compounds[1] or forming low-dimensional nanostructured materials.[3−12]

For a semiconductor to be used in solar-energy conversion, its electronic band structure is one of the most important parameters and determines, among others, the range of the solar spectrum it can absorb. Because of their relatively simple structure and the ease to form well-defined surfaces, electronic properties of the TMDC materials, in general, and the MoS_2 family, in particular, have been intensively studied by direct and inverse photoemission spectrum (PES/IPS),[13−24] various optical absorption spectroscopic techniques,[25−29] and electrochemical and photoelectrochemical measurements.[30,31] Molybdenum and tungsten dichalcogenides are characterized by partial occupation of M-d orbitals. A band gap forms between occupied and unoccupied d states as a result of ligand-field splitting, and the top valence band states are dominated by d_{z2} character. This is advantageous since the lowest-energy electronic excitation is of an intra-atomic nature so that these compounds are resistive against photocorrosion, in contrast to CdS and CdSe.[32] This qualitative picture is further supported by more elaborate first-principles analysis,[17] which indicates that the highest occupied states in these materials are actually of antibonding character, and therefore, the creation of a hole at the valence band maximum by photoexcitation strengthens the M−X bonding.

Partly due to the need to interpret experimental data, various theoretical approaches have also been used to study electronic band structures of these materials.[1,17,22,23,33−40] Most of those studies are based on Kohn−Sham density functional theory (KS-DFT) in local-density or generalized gradient approximations (LDA/GGA). KS-DFT with LDA/GGA suffers from the well-known band gap problem; that is, the band gaps of insulating materials as obtained from Kohn−Sham single-particle energies are systematically underestimated with respect to experimental fundamental band gaps measured from PES and IPS.[41] Indeed, for the MoS_2 family, the LDA/GGA KS gaps are typically underestimated by nearly 30%. Although recent years have seen a lot of efforts to solve the band gap problem

Received: January 3, 2012
Revised: March 9, 2012
Published: March 13, 2012

within the DFT framework (see, e.g., refs 42 and 43, and the references therein), no general and accurate approaches have been developed yet.

A theoretically rigorous way to solve the band gap problem is to go beyond the KS-DFT framework by formulating the electronic band structure in terms of the single-particle Green's function (G).[41,44,45] Many-body perturbation theory in the GW approximation[46] is currently the most accurate first-principles approach to describe the electronic band structures of crystalline systems, and its performance for simple sp-bonded semiconductors has been well established since the 1980s.[47−49] On the other hand, despite the importance of the TMDC materials and the extensive PES and optical spectroscopic studies, they have been rarely studied by the GW approach.[12,50] In a recent work,[50] we have investigated electronic properties of four simplest TMDC materials, zirconium and hafnium disulfide and diselenide (the ZrS_2 family), by the GW approach, and we have found very good agreement between the GW prediction and experiment. In this work, we extend the study to the MoS_2 family of compounds, which are scientifically more interesting and theoretically more challenging considering their d states characters of their valence and conduction bands. Besides the electronic band structure of bulk materials, we also investigate absolute band positions, that is, the energy of the valence band maximum and conduction band minimum with respect to the vacuum level, which are crucial parameters for the application of these materials in solar-energy conversion.[32]

The paper is organized as followings. In the next section, we give an overview of the theoretical methods used in this work, including the basic ideas of the GW approximation for electronic band structure, the approach used for the determination of absolute band positions, and some computational details. The third section presents our main results with a detailed comparison with available experimental data, and discusses the implications of our findings for solar-energy conversion. The fourth section closes the paper by summarizing our main results.

THEORY AND METHOD

Electronic Band Structure from the *GW* Approximation. Electronic band structure is one of the most fundamental properties of a semiconductor that has far-reaching influences on various physical and chemical properties of the material. Experimentally, it can be probed straightforwardly by direct and inverse photoemission spectroscopy (PES/IPS).[51] In PES, electrons are excited by photons of a given energy out of the sample surface, and by measuring their energy distribution, the information of occupied states can be revealed. In IPS, a reversed process is measured: Electrons of a certain energy are injected into the sample, filling into the unoccupied states of the system, and the redundant energy is released as photons, whose energy distribution gives the information of the unoccupied states. Theoretically, such processes can be described in the so-called quasi-particle (QP) picture,[41,44] in which either a hole (PES) or an electron (IPS) quasi-particle is created. Although apparently a single-particle process, QP excitations are truly many-body quantities due to electron−electron (e−e) interactions. For semiconductors, the most important interaction effect is the screening, that is, the weakening of effective interaction between electrons as a result of the presence of other electrons.[44] Since the dynamic aspect of screening plays an important role in common semiconductors, all static mean-field approaches, including Hartree−Fock or Kohn−Sham single-particle equations, cannot describe QP excitations in a satisfactory way.[41]

A rigorous theoretical framework for QP excitations can be obtained from many-body perturbation theory based on the one-body Green's function (GF) G,[44,52] in which the central quantity is the so-called exchange-correlation self-energy that accounts for all nonclassical dynamical electron interaction effects beyond the Hartree approximation.[41,44−49] In principle, the self-energy can be obtained exactly by solving a set of integro-differential equations, first formulated in a complete way by Hedin,[46] which are, however, too complicated to solve even for the simplest systems, such as the homogeneous electron gas. Further approximations have to be introduced, and the most widely used one is the so-called GW approximation in which the self-energy is simply the product of G and the screened Coulomb interaction W, the latter being in the random-phase approximation (RPA).[46] In practice, the QP energies within the GW approximation are often calculated as a first-order correction to the LDA/GGA Kohn−Sham single-particle energies, and both G and W are calculated using the LDA/GGA single-particle energies and wave functions, hence termed G_0W_0.[41,47,48] Further improvement can often be gained by including partial self-consistency in the calculation of G using QP energies, but with fixed RPA screening (W_0) (see, e.g., refs 53 and 54), which is often termed as GW_0. In this work, we use GW_0 based on the Perdew−Burke−Ernzerhof (PBE)[55] GGA single-particle Hamiltonian. We expect that using other variants of LDA or GGA as the reference for GW_0 will give similar results as far as the electronic band structures are concerned.

Determination of Absolute Band Positions. For a semiconductor that is used for such important applications as photovoltaics or photocatalysis, anther important aspect of its electronic properties is the absolute band positions, that is, the energy of the valence band maximum (VBM) and conduction band minimum (CBM) with respect to the vacuum level.[32] They are related to the ionization potential (I) and electron affinity (χ) of the material, the energy needed to remove an electron from the highest occupied state of the system and the energy radiated when filling the electron into the lowest unoccupied state, respectively. These parameters play crucial roles in determining the properties of the interface between two phases, such as heterojunctions of two semiconductors or the semiconductor−electrolyte interfaces.[32] Since the electron affinity can be readily obtained from the ionization potential and the fundamental band gap, we will mainly discuss the ionization potential henceforth. Experimentally, the ionization potential is often obtained from the work function ϕ, the minimum energy required to excite an electron from the Fermi level to vacuum, and the valence band upper edge with respect to the Fermi level. Figure 1 illustrates schematically the definition of these quantities and the relation between them. We note that, for metallic systems, the ionization potential is identical to the work function.

To interpret experimentally observed trends, phenomenological models are often used to estimate absolute band positions, and the most widely used is the one based on Mulliken's absolute electronegativity (EN) of atoms.[56] The latter is defined as the average of the ionization potential and electron affinity, $\phi = 1/2(I + \chi)$. On the basis of the assumption that the absolute EN of a solid-state material with the chemical formula M_mX_n can be estimated as the geometric mean of the

dx.doi.org/10.1021/jp300079d | J. Phys. Chem. C 2012, 116, 7664−7671

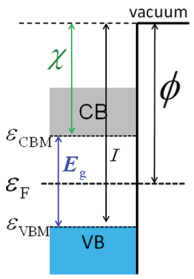

Figure 1. Schematic illustration of absolute band positions with respect to the vacuum level.

ENs of the constituent atoms,[57] the ionization potential of M_mX_n can be estimated as

$$I^{(\mathrm{EN})} = [\phi(\mathrm{M})^m \phi(\mathrm{X})^n]^{1/(m+n)} + \frac{1}{2}E_g \quad (1)$$

For simple binary semiconductors, the EN model predicts the ionization potentials in remarkably good agreement with experiment.[57] Nevertheless, the general applicability of the EN model is difficult to establish, and its validity for more complicated materials is still not clear.

The ionization potential can also be obtained from first-principles calculations by constructing a slab model that is sufficiently thick and with a large enough vacuum region.[58,59] The ionization potential can be obtained from the difference between the electrostatic potential in the vacuum region (V_{vac}) and the KS band energy at the valence band maximum (ε_{VBM}), both obtained from the same slab model calculation[58]

$$I^{(\mathrm{KS})} = V_{vac} - \varepsilon_{VBM} \quad (2)$$

The slab model has been used to calculate the work functions of many metals with generally good agreement with experiment.[60] For insulating systems, the validity of the slab model for ionization potentials needs some close scrutiny. For molecular systems, it is well known that the minus of the highest occupied molecular orbital (HOMO) energy in LDA/GGA is a very poor approximation of the ionization potential due to the self-interaction error in the LDA/GGA xc potential. We can, therefore, expect that the ionization potentials of semiconductors from the slab model alone is likely inadequate. Considering the success of *GW* for band gaps, it is highly desirable to include *GW* corrections also in the slab model calculation of the ionization potential. A direct *GW* treatment of the slab model, however, poses a formidable computational challenge. A relatively simpler scheme is to add the *GW* correction to the VBM ($\Delta\mathcal{E}_{VBM}^{(bulk)}$) obtained from the bulk system to eq 2

$$I^{(GW\text{-VBM})} = V_{vac} - \varepsilon_{VBM} - \Delta\mathcal{E}_{VBM}^{(bulk)} \quad (3)$$

termed henceforth as the *GW*-VBM scheme.

Carter and co-workers recently proposed an alternative *GW* correction scheme based on the assumption that, although KS-DFT with LDA/GGA or other more generalized approximate xc functionals cannot describe the band gaps and ionization potentials accurately, it can nevertheless give the band gap center (BGC), that is, the average of the energies at VBM and CBM, very well.[61] The *GW* corrected ionization potential can then be obtained as

$$I^{(GW\text{-BGC})} = \left[V_{vac} - \frac{1}{2}(\varepsilon_{VBM} + \varepsilon_{CBM})\right] + \frac{1}{2}E_g^{GW} \quad (4)$$

where E_g^{GW} is the *GW* fundamental band gap of the bulk system. From a practical point of view, the *GW*-BGC scheme has the advantage that E_g^{GW} is computationally easier to converge than $\Delta\mathcal{E}_{VBM}^{(bulk)}$ with respect to such important parameters as the size of the basis and the number of unoccupied states in *GW* calculations.[53,62] In this work, we will report results from both *GW* correction schemes. A systematic comparison of the two approaches is going to be reported elsewhere.

Computational Details. In this work, all DFT calculations are performed employing the WIEN2k package[63] in which Kohn–Sham DFT equations are solved in the full-potential linearized augmented plane-wave (FP-LAPW) approach, currently one of the most accurate implementations of the Kohn–Sham DFT method for crystalline systems.[64] The following parameters are used for the FP-LAPW basis: the muffin-tin (MT) radii R_{MT} are 2.15 Bohr for Mo and W, and 2.0 Bohr for S and Se; the LAPW basis functions with the angular quantum number l up to l_{max} = 10 in the MT region, and the plane-wave energy cutoff determined by min $R_{MT} \times K_{max}$ = 7.0 in the interstitial (IS) region are used for the representation of Kohn–Sham orbitals; the electron density and the KS effective potential are expanded by lattice harmonics with l up to l_{max} = 4 within the MT spheres, and by plane waves in the IS region. The Brillioun zone is sampled by a k-mesh of 12 × 12 × 2, corresponding to 38 k-points in the irreducible Brillouin zone.

GW calculations are performed using the FHI-gap (Green-function with Augmented Plane waves) package, a newly developed all-electron *GW* code interfaced to WIEN2k.[65] The Brillouin zone is sampled by a k-mesh of 6 × 6 × 1; unoccupied states with an energy up to ∼160 eV are taken into account. Densities of states (DOS) are calculated using a k-mesh of 18 × 18 × 4. The *GW* DOS are obtained from *GW* quasi-particle energies, first calculated on the sparse-mesh and then interpolated to the fine k-mesh using the Fourier interpolation technique.[66] A Gaussian broadening of 0.3 eV was chosen to roughly mimic typical experimental resolutions. Spin–orbit coupling is taken into account perturbatively.[50]

For the evaluation of absolute band positions, we construct a periodic slab model that is made of a symmetric 6-MX_2-layer slab separated by a vacuum layer of 15 Å. The central two MX_2 layers are fixed to their bulk positions, and the surface layers are relaxed along the normal direction using the PBE for solids (PBEsol) GGA functional, which has been shown to be able to describe the weak interlayer interactions in TMDC materials accurately.[50] The surface relaxation of these materials is actually very small due to the weak interlayer interactions. The ionization potential is then calculated according to eqs 2–4. Using the *GW* fundamental band gap, we can then obtain the values of the electron affinity as well.

RESULTS AND DISCUSSIONS

Crystal Structures. At room temperature and normal pressure, molybdenum and tungsten dichalcogenides (MoX_2 and WX_2) crystallize in the 2Hb-MoS_2 structure (Figure 2), in which M(=Mo or W) atoms fall in the center of the trigonal

dx.doi.org/10.1021/jp300079d | J. Phys. Chem. C 2012, 116, 7664–7671

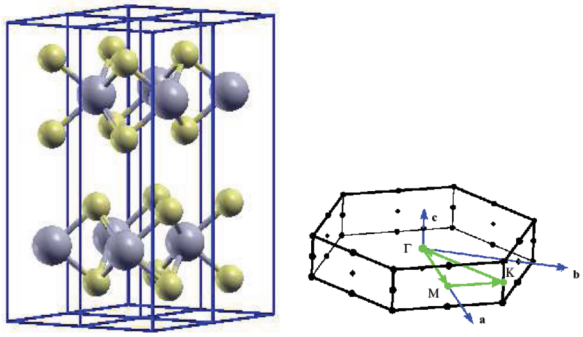

Figure 2. Left: illustration of the 2Hb-MoS_2 structure where the big and small balls represent M(=Mo or W) and X (=S or Se) atoms, respectively. Right: the corresponding Brillouin zone where the **k** path used to plot the band structure diagram is also shown.

prismatic coordination. The MX_2 sandwich layers repeat along the normal direction with a periodicity of two layers, leading to a global symmetry of *P*63/*mmc* type (space group No. 194). The primitive unit cell contains two units of chemical formula MX_2 ($Z = 2$), in which M atoms occupy the 2c sites ((1/3, 2/3, 1/4) and (2/3, 1/3, 3/4)), and X atoms occupying 4f sites ((1/3, 2/3, u), (2/3, 1/3, 1/2 + u), (1/3, 2/3, 1/2 − u), and (2/3, 1/3, −u)). To facilitate the comparison with experiment, we use experimental structural parameters, as collected in Table 1, for all the calculations in this work.

Table 1. Lattice Constants *a* and *c* (in Units of angstroms) and the Internal Coordinate *u* Used in the Calculations

materials	*a*	*c*	*u*	source
MoS_2	3.169	12.324	0.123	ref 67
$MoSe_2$	3.289	12.927	0.121	ref 68
WS_2	3.153	12.323	0.123	ref 68
WSe_2	3.282	12.961	0.121	ref 68

Band Gaps. Table 2 collects the band gaps obtained from PBE-GGA and *GW* calculations, together with experimental gaps obtained from different measurements, mainly extracted from optical absorption spectroscopic data. Rigorously speaking, the band gaps calculated from *GW* should be compared to those obtained from PES and IPS measurements since the band gaps from optical absorption data may contain the contribution of electron−hole interaction (excitonic effects). However, for indirect fundamental gaps, the excitonic effects are expected to be small.[27] This is confirmed by the fact that, for WSe_2, both optical absorption experiments[27,29,30] and PES+IPS[21,22] give essentially same indirect gap (∼1.2 eV). For optical transitions occurring at the direct gaps, excitonic effects may become significant, and therefore, more caution is needed when comparing theory and experiment.

Table 2. Minimal Indirect ($E_g^{(i)}$) and Direct ($E_g^{(d)}$) Band Gaps (in Units of eV) of MX_2 (M = Mo and W; X = S and Se) from PBE, *GW*, and Experiment[a]

materials		PBE	*GW*	expt
MoS_2	$E_g^{(i)}$	0.88	1.23	1.22,[26] 1.23[69]
	$E_g^{(d)}$	1.62	2.07	1.77,[26] 1.74[69]
$MoSe_2$	$E_g^{(i)}$	0.84	1.11	1.10,[26] 1.12[27]
	$E_g^{(d)}$	1.39	1.83	1.38[26,69]
WS_2	$E_g^{(i)}$	0.94	1.30	1.34,[26] 1.35,[69] 1.39,[28] 1.42,[70] 1.40[18]
	$E_g^{(d)}$	1.65	2.13	1.78,[26] 1.79,[69] 1.81,[28] **2.01**,[18] **2.10**[25]
WSe_2	$E_g^{(i)}$	0.92	1.19	1.17,[29] 1.27,[30] 1.22,[27] **1.2**,[21] **1.3** ± 0.1[22]
	$E_g^{(d)}$	1.33	1.75	**1.75**[25]

[a]Most experimental gaps are obtained from optical absorption spectroscopic data without explicit consideration of excitonic effects, and a few exceptional cases, in which the band gap is obtained either from PES+IPS or from optical absorption, but excluding the excitonic effects, are indicated as bold. See the text for detailed discussions.

We first consider the fundamental (indirect) band gaps. In general, the fundamental band gaps from PBE are about 30% smaller than the experimental values. We note that the errors of PBE for these materials are significantly smaller than those in the ZrS_2 family,[50] where a typical error of ∼70% has been observed. This can be attributed to the intra-atomic nature of the band gap in these materials: since both VBM and CBM states have similar characters (M-d), the error in the PBE band gap can be reduced by error cancellation. Similar to what we have seen for the ZrS_2 family,[50] *GW* gives band gaps all falling well within the error bar of experimental data or the uncertainty related to different experimental measurements. This is quite remarkable considering that two families of materials have rather different band characters.

The situations for the direct gaps are more complicated. In general, the minimal direct gap of an indirect-gap material is more difficult to measure accurately than the indirect gap. Most of the experimental direct gaps in Table 2 are extracted by fitting the optical absorption coefficient $\alpha(\omega)$ as a function of incident photon energy in terms of the relation $\omega\alpha(\omega) \sim (\omega - E_g)^{1/2}$.[71] The accuracy of this approach can be limited by several factors. From a physical point of view, the relation used for fitting is obtained by assuming a highly simplified two-band model without considering excitonic effects.[71] From a practical point of view, for an indirect-gap material, the contributions from direct and indirect absorptions overlap in the total absorption so that a unique determination of the direct absorption edge is not straightforward. In some rare cases, excitonic effects are taken into account explicitly when extracting the direct gaps from experimental data (indicated in Table 2 as bold). In an optical study of WS_2 reported in ref 18, two excitonic peaks are observed at 1.95 and 2.36 eV, and by assuming the excitonic binding energy of 0.06 eV, the authors estimated the direct gap of WS_2 to be 2.01 eV, which is about 0.2 eV larger than those obtained from the fitting approach. In ref 25, the influences of excitonic effects on the absorption edge was considered by fitting the experimental imaginary dielectric function in terms of a Lorentzian oscillator model. By assuming that the direct gap corresponds to the exciton series limit, the direct gaps of WSe_2 and WS_2 are obtained as 1.75 and 2.10 eV, respectively.

Comparing *GW* and experiment, we can see that, in general, the *GW* direct gaps are consistently larger than the experimental ones obtained from direct fitting of the absorption data by about 0.3−0.4 eV, but are very close to those experimental data[18,25] in which excitonic effects are already excluded. The latter, together with the overall good agreement between *GW* and experiment for the indirect gaps, indicates that *GW* can describe both direct and indirect gaps of these materials very well and that the apparent discrepancies between *GW* results and many widely cited experimental direct gaps can be attributed to the inadequacy in the way that direct gaps are extracted from optical absorption data. A more rigorous verification requires incorporating excitonic effects directly by

dx.doi.org/10.1021/jp300079d | J. Phys. Chem. C 2012, 116, 7664−7671

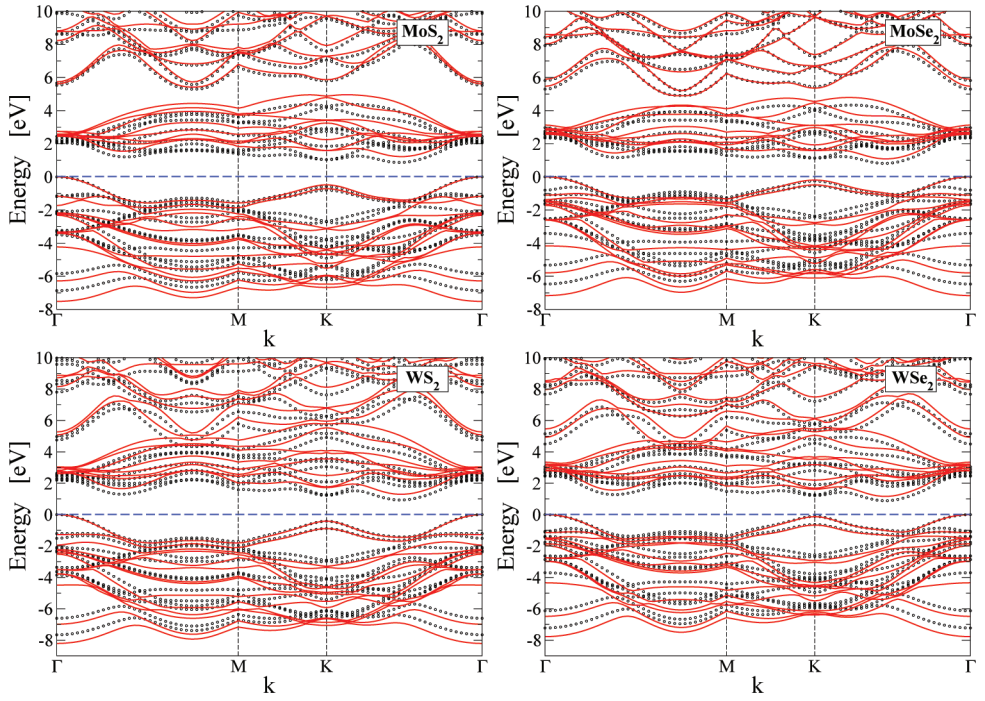

Figure 3. Band structures of MoS_2, $MoSe_2$, WS_2, and WSe_2 from PBE (dots) and *GW* (solid lines). The energy at the valence band maximum is taken as zero.

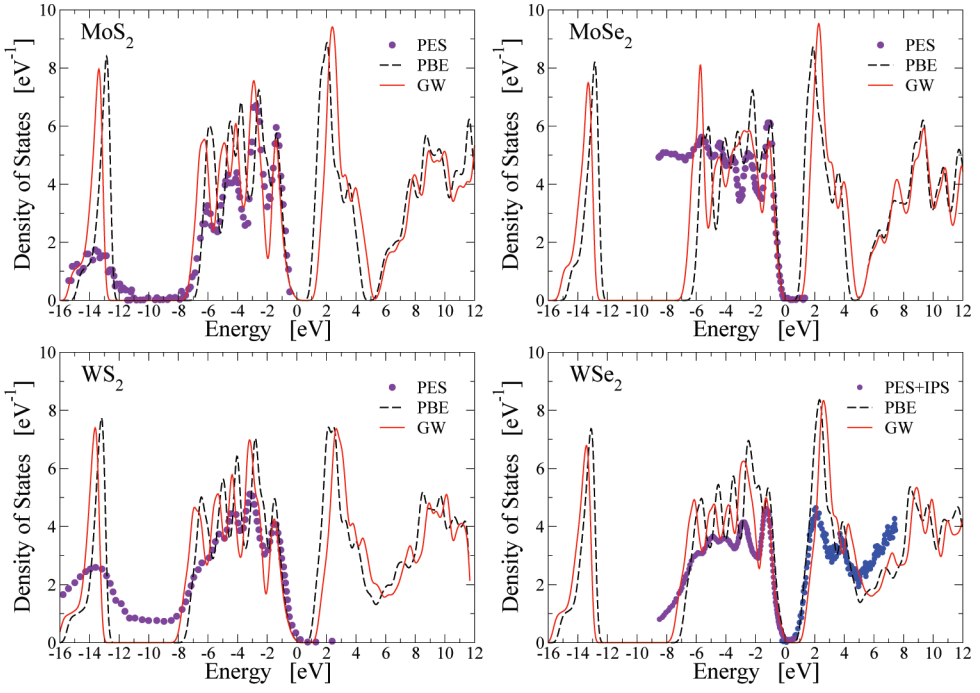

Figure 4. Density of states of MoS_2, $MoSe_2$, WS_2, and WSe_2 obtained from PBE KS orbital energies and GW quasi-particle energies. The energy at the valence band maximum is taken as zero. X-ray photoemission spectral data, extracted from refs 16, 13, 73, and 22 for MoS_2, $MoSe_2$, WS_2, and WSe_2, respectively, and the IPS data extracted from ref 22 are also plotted for comparison.

solving the Bethe−Salpeter equation, which treats electron−hole interaction based on the quasi-particle spectrum as described by *GW*.[72]

Band Structures. Figure 3 shows the band structure of MoS_2, $MoSe_2$, WS_2, and WSe_2 obtained from the PBE-GGA and *GW*, with the energy of their respective VBM taken as zero. Consistent with previous theoretical studies,[22,23,35−38,40] all of these four materials have an indirect minimal gap, with the VBM located at the Γ ($\mathbf{k}$ = (0, 0, 0)), and the CBM at the middle point between K ($\mathbf{k}$ = (1/3, 1/3, 0)) and Γ. The minimal direct gap occurs at K.

Comparing the PBE and *GW* band structures, we can see that, in general, the dependence of QP corrections on $\mathbf{k}$ vectors is rather weak so that the PBE band structures differ from the *GW* ones by essentially a rigid shift. However, the magnitude of the QP corrections does depend on the energy or, more

dx.doi.org/10.1021/jp300079d | J. Phys. Chem. C 2012, 116, 7664−7671

Table 3. Ionization Potentials (in Units of eV) of MX_2 (M = Mo and W; X = S and Se) Obtained from the Slab Model Calculations and from the Electronegativity Model[a]

materials	PBE	*GW*-VBM	*GW*-BGC	EN	expt	atom	*I*	*A*
MoS_2	5.33	5.22	5.45	5.96	5.47 ± 0.15[b]	S	10.36	2.08
$MoSe_2$	4.98	4.85	5.08	5.71		Se	9.75	2.02
WS_2	5.14	5.18	5.26	6.19		Mo	7.10	0.75
WSe_2	4.83	4.85	4.91	5.94	5.19 ± 0.1[b]	W	7.98	0.82

[a]Atomic ionization potentials and electron affinities (in units of eV) used in the EN model are taken from ref 74, also collected in the table. [b]Reference 75.

precisely, the characters of the states. For valence bands, the quasi-particle correction increases as the binding energy of the states increases, leading to a noticeably larger valence bandwidth than the PBE ones. For unoccupied states, the QP corrections for low-lying conduction bands that are mainly of d character are considerably larger than those for high-lying conduction bands that are mainly cationic-s character. We note that the difference between two types of conduction bands is stronger in MoX_2 that in WX_2. Such a dependence on the characters of the states is fully consistent with the general features of *GW*: the *GW* corrections with respect to LDA/GGA single-particle energies are more significant for states with stronger localized characters for which the self-interaction errors of LDA/GGA is more severe.

It is also interesting to compare band structures of sulphides and selenides. While in MoS_2, the energy of the top valence band state at K is about 0.5 eV lower than that at Γ, the difference is reduced to about 0.2 eV in $MoSe_2$. Similar features also occur in WS_2 and WSe_2. For WSe_2, the small difference (∼0.2 eV) in top valence band energies between Γ and K may explain the discrepancy between theoretical results and the experimental observation about the location of the VBM.[22] The limited resolution in those experiments may make it difficult to differentiate such a small difference.

Another interesting feature as revealed by Figure 3 is about the difference between MoX_2 and WX_2. Although their band gaps are nearly same, the position of the low-lying conduction bands, mainly of d character, differs strongly: in MoX_2, these unoccupied d states are essentially separated from high-lying conduction bands, but in WX_2, two types of conduction bands nearly merge with each other. This feature, together with the difference in *GW* corrections we have mentioned before, indicates that the chemical bonding differs in MoX_2 and WX_2. The latter is further demonstrated in the Supporting Information. In particular, Figure S1 (Supporting Information) shows the contour plot of the electron density difference, that is, the difference between the electron density of the crystalline system and the overlap of the densities of free atoms, of MoS_2 and WS_2. Figure S2 (Supporting Information) shows the comparison of the projected density of states of MoS_2 and WS_2. In both cases, MoS_2 and WS_2 exhibit noticeably different features.

Density of States. Figure 4 shows the density of states (DOS) of MoS_2 and $MoSe_2$ obtained from PBE-GGA and *GW*. Some of the differences between PBE and *GW* are already mentioned when we discuss band structure diagrams in the preceding section, but they are shown in these DOS plot more explicitly: (1) the valence bandwidth is increased by *GW* corrections slightly by about 0.8 eV, (2) the splitting between Mo-d_z^2 and chalcogen-p states is noticeably enhanced, which can be more clearly seen from the projected density of states plot shown in Figure S3 (Supporting Information), and (3) the chalcogen s states located at ∼ −13 eV are shifted toward lower energy ∼0.7 eV.

In Figure 4, we also collect the representative experimental X-ray photoemission (XPS) data for these materials, and for WSe_2, the IPS data for unoccupied states as well. Since the Fermi energy used as the energy zero in experimental data is determined by extrinsic factors, such as the doping level of the sample or the Fermi energy of the metallic substrate used in the PES/IPS measurements, which is inaccessible by theoretical calculations of perfect crystals, we have realigned experimental data with theoretical DOS so that first peak below VBM matches. With this alignment, we can see that the *GW* DOS can reproduce all main features observed in XPS, and the positions of main peaks agree very well. That is true also for S-3s semicore states in MoS_2 and WS_2, similar to what we have observed in previous studies of HfO_2 and ZrO_2[54] and the ZrS_2 family of TMDC materials.[50] For WSe_2, the IPS data for unoccupied states are also measured and are plotted in Figure 4. We can see again that the two peaks at ∼2 and ∼4 eV as well as the rise at ∼6 eV are all well reproduced by *GW* DOS.

Absolute Band Positions. Table 3 shows the ionization potentials of the four TMDC materials obtained from the slab model calculations without and with *GW* corrections, and from the electronegativity model (using the *GW* band gaps in eq 1), respectively. For MoS_2 and WS_2, we also collect the experimental values of the ionization potentials obtained from PES measurements.[75] For these materials, the *GW* corrections to VBM energies are very small and even become positive for MoS_2 and $MoSe_2$. This could be due to numerical errors related to the inadequate convergence that can be reached in the current *GW* calculations, but it can also be related to the systematic error of *GW* for the binding energy of states with strong d or f characters.[53,76,77] As a result, the *GW*-VBM scheme gives ionization potentials that are either very close to (for WS_2 and WSe_2) or slightly smaller (for MoS_2 and $MoSe_2$) than those from PBE. On the other hand, the ionization potentials from *GW*-BGC are always larger than those of PBE by about 0.1−0.2 eV. Only very rare experimental data exist for the ionization potentials of these materials. In a systematic study of band alignment of layered semiconductor heterointerfaces prepared by van der Waals epitaxy, Schlaf et al. obtained the ionization potentials of MoS_2 and WSe_2 from PES measurements.[75] In general, the results from the slab model calculations, in particular, those from the *GW*-BGC scheme, agree quite well with the available experimental data. On the other hand, the ionization potentials from the EN model are significantly larger than the slab model results and, therefore, strongly deviate from experimental values, indicating that the EN model is not valid for this type of material. In general, the failure of the EN model is expected since it is purely based on atomic parameters without taking into account any specific characters of chemical bonding.

dx.doi.org/10.1021/jp300079d | J. Phys. Chem. C 2012, 116, 7664−7671

To see the implication of our theoretical results for photosplitting of water, we show in Figure 5 the energies of

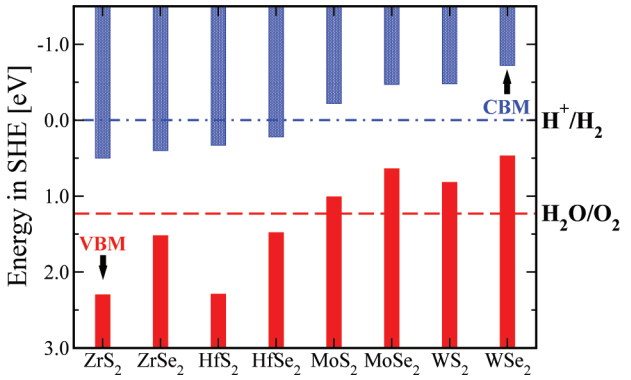

Figure 5. Theoretical band positions of MX_2 (M = Zr, Hf, Mo, and W; X = S and Se) in the standard hydrogen electrode (SHE) scale obtained from the *GW*-BGC scheme. The redox potentials for water reduction (H^+/H_2) and oxidation H_2O/O_2 are also shown for comparison.

VBM and CBM of MX_2 (M = Zr, Hf, Mo, and W; X = S and Se), obtained from the slab model within the *GW*-BGC scheme, together with the redox potentials for the reduction and oxidation of water (H^+/H_2 and H_2O/O_2), all in the standard hydrogen electrode (SHE) scale. The latter is related to the absolute vacuum scale by −4.44 eV.[32] For a semiconductor to work as a photocatalyst for H_2 (O_2) evolution, its CBM (VBM) has to be more negative (positive) than the redox potential of H^+/H_2 (H_2O/O_2) in the SHE scale. The most remarkable feature shown in Figure 5 is that the positions of VBM and CBM with respect to water oxidation and reduction redox potentials are exactly opposite for the MoS_2 family and for the ZrS_2 family, implying that, whereas the ZrS_2 family can only be used for water oxidation (H_2O/O_2), the MoS_2 family can only be used for water reduction (H^+/H_2), and therefore, none of them can be used as the photocatalyst for overall splitting of water to produce H_2 and O_2 simultaneously. Among all of these materials, MoS_2 is a little special in the sense that its VBM and CBM are close to the water oxidation and reduction potentials, respectively, in particular, in terms of the results from the *GW*-BGC scheme. On the other hand, the bulk MoS_2 material is not appropriate to be used as a photocatalyst for overall water splitting because its band gap is too small compared with the optimal band gap of ∼1.8 eV. It has been reported that the band gap of MoS_2 can be tuned by forming nanostructures.[3−5] Nanostructured MoS_2 is, therefore, promising to be used as the working material for solar-driven overall water splitting or other environmentally important photocatalytic systems.[5]

CONCLUSIONS

In this paper, we have investigated electronic properties of molybdenum and tungsten disulfide and diselenides by many-body perturbation theory in the *GW* approximation. We have found that the fundamental (indirect) band gaps of all of these materials can be well described by the *GW* approach. For minimal direct gaps, the *GW* results are systematically larger than the experimental data that are obtained by simplistic fitting of absorption coefficients, but agree very well with those that have taken into account excitonic effects explicitly, indicating that the consideration of the latter are important to extract reliable experimental direct band gaps. We also found very good agreement between the calculated density of states from *GW* quasi-particle band energies and the photoemission spectroscopic data. By combining GGA calculations of the slab model with the *GW* corrections for bulk systems, we have also calculated ionization potentials of these materials, which are then compared to the results obtained from the phenomenological EN model and available experimental data. For MoS_2 and WSe_2, whose valence band positions have been determined experimentally, the *GW*-corrected ionization potentials agree with experimental data reasonably well. In general, the EN model gives ionization potentials that are significantly larger than those from *GW*, indicating that the estimation based on such a phenomenological model can be, at best, qualitative. On the basis of our theoretical findings, we predict that these materials in their pristine form are not suitable to be used as the photocatalyst for overall photosplitting of water because their VBM and CBM energies do not match the redox potentials of water oxidation and reduction, which, however, can be changed by forming nanostructures, especially for MoS_2.

ASSOCIATED CONTENT

Supporting Information

Information on the comparison between MoS_2 and WS_2 for the difference in their chemical bonding, and the comparison of the projected density of states of MoS_2 from PBE and GW. This material is available free of charge via the Internet at http://pubs.acs.org.

AUTHOR INFORMATION

Corresponding Author

*E-mail: h.jiang@pku.edu.cn.

Notes

The authors declare no competing financial interest.

ACKNOWLEDGMENTS

This work is partly supported by the National Natural Science Foundation of China (Projects No. 20973009 and 21173005).

REFERENCES

(1) Friend, R. H.; Yoffe, A. D. *Adv. Phys.* **1987**, *36*, 1−94.
(2) Oriakhi, C. O.; Lerner, M. M. In *Handbook of Layered Materials*; Auerbach, S. M., Carrado, K. A., Dutta, P. K., Eds.; Marcel Dekker, Inc.: New York, 2004; p 509.
(3) Thurston, T. R.; Wilcoxon, J. P. *J. Phys. Chem. B* **1999**, *103*, 11−17.
(4) Wilcoxon, J. P.; Newcomer, P. P.; Samara, G. A. *J. Appl. Phys.* **1997**, *81*, 7934−7944.
(5) Abrams, B. L.; Wilcoxon, J. P. *Crit. Rev. Solid State Mater. Sci.* **2005**, *30*, 153−182.
(6) Tenne, R.; Redlich, M. *Chem. Soc. Rev.* **2010**, *39*, 1423−1434 and references therein.
(7) Mak, K. F.; Lee, C.; Hone, J.; Shan, J.; Heinz, T. F. *Phys. Rev. Lett.* **2010**, *105*, 136805.
(8) Matte, H. S. S. R.; Gomathi, A.; Manna, A. K.; Late, D. J.; Datta, R.; Pati, S. K.; Rao, C. N. R. *Angew. Chem., Int. Ed.* **2010**, *49*, 4059−4062.
(9) Lee, C.; Li, Q.; Kalb, W.; Liu, X.-Z.; Berger, H.; Capick, R. W.; Hone, J. *Science* **2010**, *328*, 76.
(10) Coleman, J. N.; et al. *Science* **2011**, *331*, 568−571.
(11) Ramasubramaniam, A.; Naveh, D.; Towe, E. *Phys. Rev. B* **2011**, *84*, 205325.
(12) Ataca, C.; Ciraci, S. *J. Phys. Chem. C* **2011**, *115*, 13303−13311.

(13) Shepherd, F. R.; Williams, P. M. *J. Phys. C: Solid State Phys.* **1974**, *7*, 4427−4440.
(14) McMenamin, J. C.; Spicer, W. E. *Phys. Rev. B* **1977**, *16*, 5474−5487.
(15) McGovern, I. T.; Childs, K. D.; Clearfield, H. M.; Williams, R. H. *J. Phys. C: Solid State Phys.* **1981**, *14*, L243−L246.
(16) Abbati, I.; Braicovich, L.; Carbone, C.; Nogami, J.; Yeh, J. J.; Lindau, I.; del Pernnino, U. *Phys. Rev. B* **1985**, *32*, 5459−5461.
(17) Coehoorn, R.; Haas, C.; Dijkstra, J.; Flipse, C. J. F.; de Groot, R. A.; Wold, A. *Phys. Rev. B* **1985**, *35*, 6195−6202.
(18) Ballif, C.; Regula, M.; Schmid, P. E.; Sanjines, R.; Levy, F. *Appl. Phys. A* **1996**, *62*, 543−546.
(19) Straub, T.; Fauth, K.; Finteis, T.; Hengsberger, M.; Claessen, R.; Steiner, P.; Hüfner, S.; Blaha, P. *Phys. Rev. B* **1996**, *53*, R16152−R16155.
(20) Park, K. T.; Richards-Babb, M.; Hess, J. S.; Weiss, J.; Klier, K. *Phys. Rev. B* **1996**, *54*, 5471−5479.
(21) Traving, M.; Boehme, M.; Kipp, L.; Skibowski, M. *Phys. Rev. B* **1997**, *55*, 10392−10399.
(22) Finteis, T.; Hengsberger, M.; Straub; Fauth, K.; Claessen, R.; Auer, P.; Steiner, P.; Hüfner, S.; Blaha, P.; Vögt, M.; et al. *Phys. Rev. B* **1997**, *55*, 10400−10411.
(23) Böker, T.; Severin, R.; Müller, A.; Janowitz, C.; Manzke, R.; Voss, D.; Krüger, P.; Pollmann, J. *Phys. Rev. B* **2001**, *64*, 235305.
(24) Klein, A.; Tiefenbacher, S.; Eyert, V.; Pettenkofer, C.; Jaegermann, W. *Phys. Rev. B* **2002**, *64*, 205416.
(25) Beal, A. R.; Liang, W. Y. *J. Phys. C: Solid State Phys.* **1976**, *9*, 2459−2466.
(26) Baglio, J. A.; Calabrese, G. S.; Kamieniecki, E.; Kershaw, R.; Kublia, C. P.; Ricco, A. J. *J. Electrochem. Soc.* **1982**, *129*, 1461−1472.
(27) Kam, K.-K.; Chang, C.-L.; Lynch, D. W. *J. Phys. C: Solid State Phys.* **1984**, *17*, 4031−4040.
(28) Julien, C.; Yebka, B.; Porte, C. *Solid State Ionics* **1998**, *110*, 29−34.
(29) Hu, S. Y.; Lee, Y. C.; Shen, J. L.; Chen, K. W.; Thiong, K. K.; Huang, Y. S. *Solid State Commun.* **2006**, *139*, 176−180.
(30) Bourezg, R.; Couturier, G.; Salardenne, J.; Doumerc, J. P.; Levy, F. *Phys. Rev. B* **1992**, *46*, 15411−15415.
(31) Gujarathi, D. N.; Solanki, G. K.; Deshpande, M. P.; Agarwal, M. K. *Sol. Energy Mater. Sol. Cells* **2006**, *90*, 2630−2639.
(32) Nozik, A. J. *Annu. Rev. Phys. Chem.* **1978**, *29*, 189−222.
(33) Mattheiss, L. F. *Phys. Rev. B* **1973**, *8*, 3719−3740.
(34) Coehoorn, R.; Haas, C.; de Groot, R. A. *Phys. Rev. B* **1985**, *35*, 6203−6206.
(35) Sharma, S.; Ambrosch-Draxl, C.; Khan, M. A.; Blaha, P.; Auluck, S. *Phys. Rev. B* **1999**, *60*, 8610−8615.
(36) Voss, D.; Krüger, P.; Mazur, A.; Pollmann, J. *Phys. Rev. B* **1999**, *60*, 14311−14317.
(37) Albe, K.; Klein, A. *Phys. Rev. B* **2002**, *66*, 073413.
(38) Reshak, A. H.; Auluck, S. *Phys. Rev. B* **2005**, *71*, 155114.
(39) Li, T.; Galli, G. *J. Phys. Chem. C* **2007**, *111*, 16192−16196.
(40) Lebegue, S.; Eriksson, O. *Phys. Rev. B* **2009**, *79*, 115409.
(41) Aryasetiawan, F.; Gunnarsson, O. *Rep. Prog. Phys.* **1998**, *61*, 237−312.
(42) Baer, R.; Livshits, E.; Salzner, U. *Annu. Rev. Phys. Chem.* **2010**, *61*, 85−109.
(43) Cohen, A. J.; Mori-Sanchez, P.; Yang, W. *Science* **2008**, *321*, 792−794.
(44) Hedin, L.; Lundqvist, B. I. *Solid State Phys.* **1969**, *23*, 1−181.
(45) Jiang, H. *Acta. Phys.-Chim. Sin.* **2010**, *26*, 1017−1033.
(46) Hedin, L. *Phys. Rev.* **1965**, *139*, A796−A823.
(47) Hybertsen, M. S.; Louie, S. G. *Phys. Rev. B* **1986**, *34*, 5390−5413.
(48) Godby, R. W.; Schlüter, M.; Sham, L. J. *Phys. Rev. B* **1988**, *37*, 10159−10175.
(49) Rinke, P.; Qteish, A.; Neugebauer, J.; Scheffler, M. *Phys. Status Solidi B* **2008**, *245*, 929−945.
(50) Jiang, H. *J. Chem. Phys.* **2011**, *134*, 204705.
(51) Hüfner, S. *Photoelectron Spectroscopy: Prinples and Applications*, 3rd ed.; Springer: Berlin, 2003.
(52) Fetter, A. L.; Walecka, J. D. *Quantum Theory of Many-Particle Systems*; McGraw-Hill: New York, 1971.
(53) Shishkin, M.; Kresse, G. *Phys. Rev. B* **2007**, *75*, 235102.
(54) Jiang, H.; Gomez-Abal, R.; Rinke, P.; Scheffler, M. *Phys. Rev. B* **2010**, *81*, 085119.
(55) Perdew, J. P.; Burke, K.; Ernzerhof, M. *Phys. Rev. Lett.* **1996**, *77*, 3865−3868.
(56) Mulliken, R. S. *J. Chem. Phys.* **1934**, *2*, 782−793.
(57) Nethercot, J. N. Jr. *Phys. Rev. Lett.* **1974**, *33*, 1088−1091.
(58) Lang, N. D. *Phys. Rev. B* **1971**, *3*, 1215−1223.
(59) Bechstedt, F. *Prinples of Surface Physics*; Springer: Berlin, 2003.
(60) Skriver, H. L.; Rosengaard, N. M. *Phys. Rev. B* **1992**, *45*, 9410−9412.
(61) Toroker, M. C.; Kanan, D. K.; Alidoust, N.; Isseroff, L. Y.; Liao, P.; Carter, E. A. *Phys. Chem. Chem. Phys.* **2011**, *13*, 16644−16654.
(62) Kang, W.; Hybertsen, M. S. *Phys. Rev. B* **2010**, *82*, 085203.
(63) Blaha, P.; Schwarz, K.; Madsen, G. K. H.; Kvasnicka, D.; Luitz, J. *WIEN2k: An Augmented Plane Wave + Local Orbitals Program for Calculating Crystal Properties*; Karlheinz Schwarz, Techn. Universität Wien: Wien, Austria, 2001.
(64) Schwarz, K.; Blaha, P.; Trickey, S. B. *Mol. Phys.* **2010**, *108*, 3147−3166.
(65) Gomez-Abal, R.; Li, X.; Scheffler, M.; Ambrosch-Draxl, C. *Phys. Rev. Lett.* **2008**, *101*, 106404.
(66) Pickett, W. E.; Krakauer, H.; Allen, P. B. *Phys. Rev. B* **1988**, *38*, 2721−2726.
(67) Petkov, V.; Billinge, S. J. L.; Larson, P.; Mahanti, S. D.; Vogt, T.; Rangan, K. K.; Kanatzidis, M. G. *Phys. Rev. B* **2002**, *65*, 092105.
(68) Schutte, W. J.; De Boer, J. L.; Jellinek, F. *J. Solid State Chem.* **1987**, *70*, 207−209.
(69) Kam, K. K.; Parkinson, B. A. *J. Phys. Chem.* **1982**, *86*, 463−467.
(70) Li, S. J.; Bernede, J. C.; Pouzet, J.; Jamali, M. *J. Phys.: Condens. Matter* **1996**, *8*, 2291−2304.
(71) Yu, P. Y.; Cardona, M. *Fundamentals of Semiconductors: Physics and Materials Properties*, 3rd ed.; Springer: Berlin, 2001.
(72) Onida, G.; Reining, L.; Rubio, A. *Rev. Mod. Phys.* **2002**, *74*, 601−659.
(73) Jaegermann, F. S.; Ohuchi, W.; Parkinson, B. A. *Surf. Sci.* **1988**, *201*, 211−227.
(74) Dean, J. H., Ed. *Lange's Handbook of Chemistry*, 15th ed.; McGraw-Hill: New York, 1992.
(75) Schlaf, R.; Lang, O.; Pettenkofer, C.; Jaegermann, W. *J. Appl. Phys.* **1999**, *85*, 2732−2753.
(76) Shishkin, M.; Marsman, M.; Kresse, G. *Phys. Rev. Lett.* **2007**, *99*, 246403.
(77) Jiang, H.; Gomez-Abal, R. I.; Rinke, P.; Scheffler, M. *Phys. Rev. B* **2010**, *82*, 045108.